Research Square

Preprints are preliminary reports that have not undergone peer review.
They should not be considered conclusive, used to inform clinical practice,
or referenced by the media as validated information.

Yi-Nao-Kang Capsule ameliorates cerebral ischemia-reperfusion injury and suppresses the PERK/eIF2α/QRICH1 endoplasmic reticulum stress pathway in brain microvascular endothelial cells

Jian-Peng Xu
Second Affiliated Hospital of Guangzhou Medical University
Min-Hua Zheng
Second Affiliated Hospital of Guangzhou Medical University
Xin Du
Second Affiliated Hospital of Guangzhou Medical University
Tian Hu
Second Affiliated Hospital of Guangzhou Medical University
Qi-Hong Lv
Second Affiliated Hospital of Guangzhou Medical University
Jie Ouyang
Second Affiliated Hospital of Guangzhou Medical University
Xin-Yi Xu
Second Affiliated Hospital of Guangzhou Medical University
Yu-Hui Qiu
Second Affiliated Hospital of Guangzhou Medical University
Jia-Yi Zheng
Second Affiliated Hospital of Guangzhou Medical University
Ye-Feng Cai
Second Affiliated Hospital of Guangzhou Medical University
Shi-Jie Zhang
shijiezhang@gzucm.edu.cn

Second Affiliated Hospital of Guangzhou Medical University

Research Article

Keywords: Yi-Nao-Kang capsule, Cerebral ischemia-reperfusion injury, Brain microvascular endothelial cells, Endoplasmic reticulum stress, PERK/eIF2α/QRICH1 pathway

Posted Date: November 13th, 2026

DOI: https://doi.org/10.21203/rs.3.rs-11487946/v1

License: This work is licensed under a Creative Commons Attribution 4.0 International License.
Read Full License

Additional Declarations: No competing interests reported.

Abstract

Background

Yi-Nao-Kang (YNK), a traditional Chinese medicine formula widely used for ischemic stroke rehabilitation, is supported by long-term clinical experience, yet the evidence for its efficacy remains limited and its neurovascular protective mechanisms are undefined, prompting this mechanistic investigation.

Materials and methods

We examined the mechanism by which YNK protects against cerebral ischemia–reperfusion injury (CIRI), using an in vivo middle cerebral artery occlusion (MCAO) model in SD rats and an in vitro oxygen–glucose deprivation/reoxygenation (OGD/R) model in bEnd.3 cells. The effects of YNK on the PERK/eIF2α/QRICH1 pathway were verified by Western blotting, quantitative real time PCR (qPCR), immunofluorescence staining, biochemical analysis of oxidative stress markers and detection of inflammatory cytokines.

Results

Compared with the MCAO model group, YNK administration reduced cerebral infarct volume, improved neurological deficits, and was accompanied by reduced endoplasmic reticulum stress (ERS), downregulated endothelial and pericyte QRICH1 expression, and mitigated oxidative stress and neuronal apoptosis; in OGD/R-exposed bEnd.3 cells, the PERK inhibitor GSK2656157 produced protective and pathway-suppressing effects similar to those of YNK.

Conclusion

YNK ameliorates cerebral ischemia-reperfusion injury, and its protective effects are accompanied by suppression of PERK/eIF2α/QRICH1-mediated ERS in brain microvascular endothelial cells. Because active constituents were not identified and YNK-only control groups were not included, these findings should be considered preliminary and hypothesis-generating; further preclinical evaluation is required before clinical translation.

Introduction

Stroke remains one of the leading global causes of permanent disability and mortality, with ischemic stroke (IS) accounting for 60%-70% of all stroke cases[1]. Intravenous thrombolysis and mechanical thrombectomy are the standard acute reperfusion therapies; however, their clinical utility is limited by narrow therapeutic windows. More importantly, restored cerebral blood flow inevitably triggers cerebral

ischemia-reperfusion injury (CIRI), which can offset the therapeutic benefits of reperfusion[2, 3]. CIRI initiates a cascade of detrimental pathological events including blood-brain barrier (BBB) breakdown, excessive endoplasmic reticulum stress (ERS), and irreversible neuronal apoptosis[4]. Deciphering the core molecular cascades driving CIRI is critical to develop novel neurovascular protective strategies for reperfusion-associated secondary brain damage[5].

Modern stroke research has shifted from isolated neuronal protection toward holistic preservation of the neurovascular unit, in which brain microvascular endothelial cells (BMECs) constitute the structural and functional core of this barrier[6, 7]. BMECs sustain cerebral homeostasis through two complementary structural functions—bidirectional exchange of nutrients and metabolic waste between blood and brain parenchyma[8], and formation of the physical BBB barrier via tight junctions[9]. Endothelial injury and tight-junction disintegration are therefore regarded as the initiating event of cerebral ischemia–reperfusion injury (CIRI), increasing BBB permeability, permitting infiltration of circulating toxins and triggering cascading neuronal death[10]. BMECs also sense vasoactive mediators to regulate cerebral blood flow, and their dysfunction aggravates microcirculatory hypoperfusion after ischemic stroke[11]. As the principal cellular components of the BBB, BMECs and pericytes maintain close anatomical and functional crosstalk[12]; primary BMEC injury is thought to secondarily induce phenotypic and functional disorder of adjacent pericytes, jointly destabilizing the neurovascular unit[13]. Protecting BMECs is therefore the primary prerequisite for neurovascular-unit integrity, and pericyte phenotype was monitored here as an auxiliary index of the protective effect of YNK on the whole unit[14]. In parallel, BMECs act as immune regulators, secreting pro-inflammatory cytokines and chemokines that recruit peripheral immune cells while releasing anti-inflammatory mediators to restrain excessive neuroinflammation[15, 16]. Restoring endothelial function has thus become a promising therapeutic frontier for ischemic stroke[17].

Severe ischemic insult triggers robust ERS and activates the unfolded protein response (UPR)[18]. The UPR consists of three parallel ER membrane signaling branches: IRE1, PERK, and ATF6[19]. Under mild stress, the UPR initiates adaptive protective programs to enhance ER folding capacity, reduce global protein synthesis, and clear misfolded proteins to restore ER homeostasis and cell survival[20]. Nevertheless, persistent, overwhelming ERS switches the UPR from pro-survival to pro-apoptotic signaling. Moderate PERK pathway activation phosphorylates eIF2α to suppress general protein synthesis and alleviate ER overload; prolonged PERK/eIF2α signaling drives transcriptional upregulation of CHOP and initiates programmed cell death[21, 22]. QRICH1 is a downstream transcriptional effector of the PERK–eIF2α branch of the unfolded protein response; multi-omics and functional studies show that it amplifies ER protein influx, aggravates proteotoxic aggregation and dictates cell fate under unresolved ERS [23]. However, whether the PERK/eIF2α/QRICH1 axis is activated in brain microvascular endothelial cells (BMECs) after cerebral ischemia, and whether it can be engaged pharmacologically, has not been established. This gap is clinically relevant because YNK is already used for ischemic stroke yet its endothelial mechanism remains undefined; determining the endothelial pathway through which YNK acts is therefore a prerequisite for its rational clinical use.

Yi-Nao-Kang capsule (YNK) is a classic multi-component traditional Chinese medicine (TCM) formula widely applied in clinical rehabilitation of ischemic stroke, formulated under the core TCM theories of “qi deficiency, blood stasis, phlegm stagnation and collateral obstruction”. Clinical experience and preliminary pharmacological reports suggest that it improves post-stroke neurological recovery and possesses anti-inflammatory, antioxidant and anti-apoptotic bioactivities. YNK comprises seven medicinal materials: *Astragalus mongholicus* Bunge (Fabaceae), *Ligusticum chuanxiong* Hort. (Apiaceae), processed *Arisaema erubescens* (Wall.) *Schott* (Araceae), processed *Gastrodia elata Blume* (Orchidaceae), *Leonurus japonicus* Houtt. (Lamiaceae), Scorpion (animal source: *Olivierus martensii* (Karsch, 1879), family Buthidae), and processed *Pinellia ternata* (Thunb.) *Makino*. The Latin binomials of all plant materials were validated via the Medicinal Plant Names Services (MPNS) and Plants of the World Online (POWO, accessed 29 December 2025); zoological authentication of the scorpion raw material was verified using the Global Biodiversity Information Facility (GBIF). Consistent with TCM holistic compatibility principles, the formula exerts combined effects of tonifying qi, activating blood circulation, resolving phlegm and unblocking collaterals, which provides a theoretical basis for its antioxidant, anti-inflammatory and ERS-modulating effects against cerebral ischemia. Previous work established an HPLC fingerprint of YNK and quantified four quality-control marker compounds, but this analysis does not identify the constituents responsible for its neurovascular effects, and the molecular mechanism underlying its endothelial protective activity remains unclear.

In this study we asked whether YNK protects the neurovascular unit, and BMECs in particular, by suppressing PERK/eIF2α/QRICH1-mediated ERS. We combined in vivo MCAO rats with in vitro bEnd.3 OGD/R models, using a pharmacological PERK inhibitor as a positive control, and also assessed downstream antioxidant, anti-inflammatory, anti-apoptotic and synaptic endpoints. Because genetic loss-of-function was not performed, these experiments test association and pharmacological dependence rather than proving that QRICH1 is required.

Materials and Methods

2.1 Experimental Animals and MCAO Model Establishment

2.1.1 Experimental Animals

140 male adult SD rats (250–310 g) were housed individually in ventilated cages at the Animal Experiment Center of Guangzhou University of Chinese Medicine. The study was approved by the Animal Ethics Committee of Guangzhou University of Chinese Medicine (Approval No. 20251201003) and followed the National Institutes of Health Guide for the Care and Use of Laboratory Animals.

2.1.2 MCAO Model Establishment

Focal cerebral ischemia was induced in rats using the intraluminal filament occlusion method. Rats were anesthetized with 3% isoflurane; a monofilament nylon suture was inserted into the internal carotid artery to occlude the middle cerebral artery for 90 min, followed by filament removal to initiate

reperfusion[24]. Sham-operated rats received identical surgical procedures without filament insertion or arterial occlusion.

2.2 Animal Groups

Rats received 7 consecutive days of intragastric pre-administration with low- or high-dose YNK prior to MCAO surgery (the Sham and Model groups received an equal volume of normal saline). After MCAO modeling, the rats were then assigned to 24 h and 72 h reperfusion subgroups—that is, the model rats were divided into IR24 h and IR72 h subgroups at this point. Daily administration continued until the designated reperfusion time points for tissue collection. Seven experimental groups were established (n = 20 rats per group): Sham group, IR24 h Model group, IR24 h + YNK-L (1 g/kg), IR24 h + YNK-H (3 g/kg), IR72 h Model group, IR72 h + YNK-L (1 g/kg), IR72 h + YNK-H (3 g/kg).

2.3 YNK Preparation and Drug Administration

Yi-Nao-Kang capsule (YNK, Batch No. 240903, 0.5 g per capsule) was supplied by Guangdong Provincial Hospital of Chinese Medicine. Capsule powder was dissolved in normal saline to a stock concentration of 0.25 g/mL, with dosages calculated according to standard interspecies pharmacokinetic conversion formulas. YNK quality was strictly controlled via HPLC quantification of four characteristic marker compounds (leonurine hydrochloride, ferulic acid, calycosin glucoside, ononin), with a batch similarity index of 0.96 matching previous published fingerprint data. YNK was administered intragastrically once daily: all rats received 7 days pre-surgical pretreatment, and dosing continued daily after reperfusion until sacrifice. IR24 h groups received one additional administration at 24 h reperfusion before sampling; IR72 h groups received three consecutive daily doses post-reperfusion before tissue collection. This unified pre-operative dosing baseline eliminated confounding variation in administration duration. HPLC fingerprint and quantification data for four quality-control marker compounds of YNK, supporting quality control and batch consistency, are presented in Supplementary Figs. S1–S5, Tables S1–S3 and Supplementary Data S1, as previously reported[25].

2.4 Antibodies and Reagents

Primary antibodies used in this study were as follows: QRICH1 (#NBP1-82196) and CD31 (#AF3628) (Novus Biologicals, USA); p-PERK (#DF7576), p-eIF2α (#AF3087), and eIF2α (#AF6087) (Affinity Biosciences, USA); PSD-95 (#ab18258) and BDNF (#ab108319) (Abcam, UK); CHOP (#T56694M) and Caspase-3 (#T40044M) (ABMART, China); PERK (#24390-1-AP), GRP78/BiP (#66574-1-Ig), BAX (#50599-2-Ig), BCL-2 (#26593-1-AP), and β-actin (#81115-1-RR) (Proteintech, China); PDI (#3501S) (Cell Signaling Technology, USA). The PERK inhibitor GSK2656157 was used as a positive control in the in vitro experiments.

2.5 Neurological Function Assessment and Cerebral Infarct Volume Measurement

2.5.1 Neurological Function Assessment

MCAO success was defined as a Zea Longa neurological deficit score of 1–3 after surgery. MCAO rats with a score of 0 or 4 were excluded from subsequent analyses. Neurological deficits were assessed by investigators blinded to group allocation using the Zea Longa and Bederson scales.

2.5.2 Cerebral Infarct Volume Measurement

Rats were euthanized after neurological assessment by intraperitoneal injection of an overdose of sodium pentobarbital (200 mg/kg). The brains were rapidly isolated and frozen at -20℃ for 20 min. The brains were coronally sectioned into 3 mm-thick slices, which were stained with 2% 2,3,5-triphenyltetrazolium chloride (TTC) solution for 15 min at room temperature in the dark. The stained slices were photographed, and the infarct volume was calculated using ImageJ software.

2.6 Histological and Biochemical Analyses

2.6.1 Nissl Staining

Brain tissues were fixed in 4% paraformaldehyde, dehydrated with gradient ethanol, embedded in paraffin, and sliced into 4 μm-thick slices containing the cortical ischemic penumbra. Slices were stained with Nissl kit (Solarbio #G1430) according to manufacturer's instructions, and images were taken using Olympus VS200 slide scanner.

2.6.2 Biochemical Assays

Cortical ischemic penumbra tissue was homogenized for biomarker detection. Commercial assay kits were used to measure tissue superoxide dismutase (SOD) activity, glutathione (GSH) concentration, malondialdehyde (MDA) content, and serum lactate dehydrogenase (LDH) release. Absorbance readings were acquired on a BioTek microplate reader following kit standard protocols.

2.7 RNA Extraction and qPCR

Total RNA was extracted from the tissue of cerebral cortical ischemic penumbra and bEnd.3 cells using TRIzol reagent (Invitrogen, USA), and the concentration and purity of RNA were quantified with a NanoDrop 2000C spectrophotometer. cDNA synthesis was performed using the Evo M-MLV RT Master Mix Kit (Accurate Biology, China), and qPCR was conducted with the SYBR Green Pro Taq HS Premix Kit (Accurate Biology, China) on the QuantStudio 7 Flex System. The relative expression of target genes was calculated via the 2^(-ΔΔCt) method, with Gapdh used as the internal reference gene. The primer sequences are listed in Table 1 and Table 2 .

Table 1
List and sequences of rat primers used for qPCR analysis. (Rattus norvegicus)

Primers	**Sequence (5'-3') (F: Forward; R: Reverse)**	**Length (bp)**
Eif2ak3	F:ACAAGGCTGTCACTCAGGTG;R:GCTAGGAGCCTTGGAGCAC	121
Eif2a	F:CACTTCAGAATGCCGGGTCT;R:AACAAGCTGACATAGGCCCC	119
Ddit3	F:ACGTCGATCATACCATGTTGAAG;R:CACTTCCTTCTGGAACACTCTCT	94
Bcl2	F:GAACTGGGGGAGGATTGTGG;R:GGGGTGACATCTCCCTGTTG	80
Bax	F:CTCAAGGCCCTGTGCACTAA;R:GGAAAGGAGGCCATCCCAG	126
Casp3	F:GAGCTTGGAACGCGAAGAAA;R:GAGTCCATCGACTTGCTTCCA	113
Qrich1	F:AAACGCAAAGTGGACATGCC;R:AGTCTGGCCTCAAAGACACG	118
Dlg4	F:TACCGCTACCAAGATGAAGACAC;R:GTTCCATTCACCTGCAACTCATA	137
Bdnf	F:TGTCGCACGGTCCCCATT;R:CCCGGTCTCATCAAAGCCTG	101
Gapdh	F:GGTACAACTCAGGTTCCGGG;R:ATCCGTTCACACCGACCTTC	142
IL1β	F:TCCAGGATGAGGACATGAGC;R:GTCGGAGATTCGTAGCTGGAT	147
IL18	F:GCTGAAGCTGAAGGCTGAAGA;R:CCTGCTGTGAAGGTGAAGGT	132

Table 2
List and sequences of mouse primers used for qPCR analysis (Mus musculus)

Primers	**Sequence (5'-3') (F: Forward; R: Reverse)**	**Length (bp)**
Eif2ak3	F:CGCGTCGGAGACAGTGTTT;R:GTCCTCCACGGTCACTTCG	97
Eif2s1	F:TCCTCGTTGCCACTAAGCAG;R:AACAAGCTGACATAGGCCCC	174
Ddit3	F:CTGGAAGCCTGGTATGAGGAT;R:CAGGGTCAAGAGTAGTGAAGGT	121
Bcl2	F:CCTGTGGATGACTGAGTACCTG;R:AGCCAGGAGAAATCAAACAGAGG	120
Bax	F:TGAAGACAGGGGCCTTTTTG;R:AATTCGCCGGAGACACTCG	140
Casp3	F:GAGCTTGGAACGGTACGCTA;R:GAGTCCACTGACTTGCTCCC	118
Qrich1	F:CGTCGCCGGAACAAAGTTAAA;R:TCCTTAGGGTTCCAGTCACCA	145
Dlg4	F:CCCCCAACATGGACTGTCTC;R:CGTTCACATATCCTGGGGCT	165
Gapdh	F:GCATCACTGCCACCCAGAAGACTG;R:ATGCCAGTGAGCTTCCCGTTCAG	153

2.8 Western Blotting

Total protein was extracted from cortical ischemic penumbra tissue, and protein concentration determined via the BCA colorimetric assay. Equal mass protein samples were separated on 10% SDS-PAGE gels, transferred to PVDF membranes (Millipore, USA), and blocked with Protein-Free Rapid Blocking Buffer (PriLeagene, China). Membranes were incubated with primary antibodies overnight at 4°C, then HRP-conjugated secondary antibodies for 1 h at room temperature. Protein bands were visualized with ECL chemiluminescent substrate (WBKLS0500, Millipore) and imaged on a Tanon 5200 chemiluminescence system. Band densitometry was quantified with ImageJ software, normalized to β-actin as loading control.

2.9 Immunofluorescence Staining

Paraffin-embedded brain tissue slices containing the cortical ischemic penumbra and cell climbing slices were fixed with 4% paraformaldehyde, permeabilized with 0.3% Triton X-100, and blocked with 5% bovine serum albumin (BSA) at room temperature for 1 h. The samples were incubated with corresponding primary antibodies at 4℃ overnight, followed by incubation with fluorescently labeled secondary antibodies at room temperature for 1 h in the dark. Subsequently, the slices were mounted with a 4',6-Diamidino-2-Phenylindole (DAPI)-containing anti-fade medium (Beyotime, China). Images were captured using an Olympus VS200 slide scanner and processed with OlyVIA software. The primary antibodies used for cell-specific immunofluorescence co-localization were as follows: PDGFRβ (#3169S, Cell Signaling Technology, USA) for pericyte labeling, CD31 (#AF3628, Novus Biologicals, USA) for endothelial cell labeling, and NeuN (#ab104224, Abcam, UK) for neuron labeling.

2.10 Cell Culture and OGD/R Model Establishment

2.10.1 Cell Culture

Mouse brain microvascular endothelial bEnd.3 cells were cultured in high-glucose Dulbecco's Modified Eagle's Medium (DMEM) complete medium supplemented with 10% fetal bovine serum (FBS) and 1% penicillin-streptomycin, and maintained in a humidified incubator at 37℃ with 5% CO_2. The medium was refreshed every 24 h.

2.10.2 OGD/R Model Establishment and Intervention Protocol

The OGD/R model was constructed to simulate the pathological process of CIRI in vitro. Briefly, cells at 70% confluence were incubated in glucose-free DMEM in a hypoxic incubator (Thermo Fisher Scientific, Forma 3131, Waltham, MA, USA; 95% N_2, 5% CO_2, 37°C) for 6 h, followed by 24 h of reoxygenation under normoxic conditions. 15% YNK-containing serum was prepared from male SD rats that received intragastric administration of 3 g/kg YNK once daily for 7 consecutive days. Blood was collected 2 h after the final administration, and serum was separated, inactivated at 56℃ for 30 min, filter-sterilized

through a 0.22 μm membrane, and stored at -80℃ until use. Blank rat serum was prepared from normal SD rats using the same method. The intervention was administered during the 6 h hypoxic period: after 6 h of hypoxia intervention, the medium was replaced with high-glucose DMEM complete medium containing 10% FBS for 24 h normoxic reoxygenation in all groups. The non-cytotoxic concentration of normal rat serum and YNK-containing serum was verified via CCK-8 assay (Supplementary Fig. S6-S7). Additional pre-experiments including the protective effect of YNK serum on cell viability after OGD, gradient DMSO cytotoxicity test, and cellular morphological observation under different treatments are presented in Supplementary Fig. S8–S10.

2.10.3 Experimental Grouping

Cells in the logarithmic growth phase were randomly divided into 4 groups (n = 6 replicates per group), with a unified total serum concentration of 15% in the intervention medium to eliminate the interference of serum concentration differences:

Control group: Cells were cultured under normoxic conditions with high-glucose DMEM containing 10% FBS + 5% blank rat serum, no OGD/R treatment;

OGD/R Model group: Cells received 6 h OGD treatment with glucose-free DMEM containing 10% FBS + 5% blank rat serum, followed by 24 h reoxygenation;

YNK-H group: Cells received 6 h OGD treatment with glucose-free DMEM containing 10% FBS + 5% YNK-containing serum, followed by 24 h reoxygenation;

GSK2656157 positive control group: Cells received 6 h OGD treatment with glucose-free DMEM containing 10% FBS + 5% blank rat serum + 1 μM GSK2656157 (dissolved in DMSO, final DMSO concentration = 0.1%), followed by 24 h reoxygenation. The final DMSO concentration of 0.1% was determined via a pre-experiment of gradient DMSO cytotoxicity, which confirmed that DMSO ≤ 0.1% had no toxic effect on bEnd.3 cells under OGD condition. In addition, a DMSO solvent-control group (OGD/R with 0.1% DMSO, YNK-free and GSK-free) was included to exclude solvent interference; its data and statistical comparison with the OGD/R Model group are presented in Supplementary Fig. S9.

2.11 Statistical Analysis

All statistical analyses were performed using GraphPad Prism 11.0 software. Data were presented as mean ± standard error of the mean (SEM) for normally distributed data, and median (interquartile range, M [P25-P75]) for non-normally distributed data. Normality of data distribution was tested via the Shapiro-Wilk test, and homogeneity of variance was tested via Levene's test.

For two-group comparisons, Student's t-test was used for normally distributed data, and Mann-Whitney U test was used for non-normally distributed data.

For multi-group comparisons, one-way Analysis of Variance (ANOVA) followed by Tukey's post-hoc test was used for data with normal distribution and homogeneity of variance; Welch's ANOVA followed by

Tamhane's T2 post-hoc test was used for data with normal distribution but unequal variance; Kruskal-Wallis H test with Bonferroni-corrected pairwise comparison was used for non-normally distributed data.

Results

3.1 YNK alleviates cerebral ischemic injury, neurological dysfunction, neuronal loss, oxidative stress and neuroinflammation in MCAO rats (Fig. 1)

To identify the optimal YNK intervention dosage and reperfusion time window against CIRI, we conducted a dose-time gradient screening experiment across seven MCAO rat groups. At both 24 h and 72 h reperfusion time points, Model group rats exhibited severe neurological deficits and markedly enlarged cerebral infarct volume relative to Sham controls (***p < 0.001 vs. Sham). High-dose YNK (YNK-H, 3 g/kg) significantly ameliorated motor neurological impairment and reduced infarct lesions. The effect of YNK-H was most evident at 72 h post-reperfusion, manifested by diminished infarct volume percentage (#p < 0.05 vs. Model, Fig. 1B, C). and lower Zea Longa neurological deficit scores (#p < 0.05 vs. Model, Fig. 1D) Nissl staining of cortical ischemic penumbra revealed extensive neuronal pyknosis and loss in Model animals, while YNK-H treatment preserved intact neuronal morphology (Fig. 1E). Based on these phenotypic screening results, 72 h reperfusion and 3 g/kg YNK-H were selected as standardized conditions for all subsequent mechanistic assays.

Biochemical detection of oxidative stress biomarkers in 72 h reperfusion cortical tissue demonstrated that Model rats displayed significantly suppressed SOD and GSH antioxidant activity (*p < 0.05, ***p < 0.001 vs. Sham), alongside elevated tissue MDA and serum LDH levels (***p < 0.001 vs. Sham).YNK-H attenuated oxidative damage, increasing SOD (#p < 0.05 vs. Model) and GSH (##p < 0.01 vs. Model) activity, reduced MDA (###p < 0.001 vs. Model) and serum LDH release (###p < 0.001 vs. Model, Fig. 1F). qPCR quantification of pro-inflammatory mediators further confirmed robust neuroinflammation in Model tissue, with marked upregulation of Il1β and Il18 mRNA (***p < 0.001 vs. Sham). YNK-H significantly suppressed transcription of both inflammatory cytokines (###p < 0.001 vs. Model, Fig. 1F), verifying the dual antioxidant and anti-inflammatory capacity of YNK against CIRI.

3.2 YNK restores impaired synaptic plasticity and inhibits neuronal apoptosis in cortical ischemic penumbra of MCAO rats (Fig. 2)

We next characterized YNK’s regulatory effects on neuronal synaptic remodeling and apoptotic cell death, two key processes governing long-term neurological recovery post-stroke. Western blot and qPCR detection of synaptic plasticity markers revealed profound downregulation of PSD-95 and BDNF protein and corresponding Dlg4, Bdnf mRNA in Model cortical tissue (***p < 0.001 vs. Sham, Fig. 2A-E). YNK-H robustly upregulated both synaptic proteins and their encoding transcripts (###p < 0.001 vs. Model). NeuN/PSD-95 double immunofluorescence confirmed diminished synaptic PSD-95 signal in ischemic neurons of Model rats; YNK-H restored abundant PSD-95 expression within NeuN-positive cortical neurons (Fig. 2F), indicating YNK enhances synaptic remodeling to facilitate functional neurological recovery after ischemia.

Apoptosis pathway detection demonstrated severe dysregulation of Bcl-2 family proteins in Model ischemic tissue: reduced Bcl-2/Bax ratio, suppressed anti-apoptotic Bcl-2 expression, and elevated pro-apoptotic Bax and executioner Caspase-3 (***p < 0.001 vs. Sham, Fig. 2G-I). YNK-H normalized apoptotic protein balance, increasing the Bcl-2/Bax ratio (##p < 0.01 vs. Model) and lowering Caspase-3 protein abundance (###p < 0.001 vs. Model). TUNEL/NeuN co-staining visualized abundant apoptotic neurons in Model ischemic penumbra; YNK-H markedly reduced the quantity of TUNEL-positive degenerative neurons (Fig. 2J). Transcriptional changes in Bcl2, Bax and Casp3 mRNA mirrored the protein-level results (Fig. 2K-M), confirming potent anti-apoptotic activity of YNK against CIRI-induced neuronal loss.

3.3 YNK suppresses PERK/eIF2α/QRICH1-mediated endoplasmic reticulum stress in MCAO rat cerebral cortex and alleviates QRICH1 overexpression in endothelial cells and pericytes (Fig. 3)

To uncover the core molecular axis mediating YNK's neurovascular protective activity, we quantified activation of the ERS PERK/eIF2α/QRICH1 cascade in cortical ischemic penumbra. Western blot analysis revealed significant upregulation of canonical ERS markers (BIP, PDI, CHOP), elevated p-PERK/PERK and p-eIF2α/eIF2α phosphorylation ratios, and increased total QRICH1 protein in Model rats relative to Sham controls (**p < 0.01, ***p < 0.001 vs. Sham, Fig. 3A-G). YNK-H treatment comprehensively blunted excessive pathway activation: reducing BIP, PDI and CHOP protein abundance (##p < 0.01 / ###p < 0.001 vs. Model), lowering PERK and eIF2α phosphorylation ratios, and suppressing QRICH1 expression (###p < 0.001 vs. Model). qPCR analysis of pathway-encoding genes recapitulated these protein-level alterations, with Model tissue exhibiting elevated Eif2ak3, Eif2a, Qrich1 and Ddit3 transcription, all significantly downregulated by YNK-H intervention (##p < 0.01, ###p < 0.001 vs. Model, Fig. 3H-K).

Single immunofluorescence staining for BIP and p-PERK visualized widespread ERS activation across the ischemic cortex of Model rats, with intense cytoplasmic fluorescent signal; YNK-H visibly attenuated BIP and p-PERK immunoreactivity (Fig. 3L). To determine the major cell population responsible for the upregulation of QRICH1 in vivo, we performed co-immunofluorescence staining of QRICH1 with the endothelial marker CD31 and the pericyte marker PDGFR-β (Fig. 3M). In the Sham brains, QRICH1 fluorescence was barely detectable in either cell type. Under ischemic conditions, however, QRICH1 fluorescence was markedly increased in CD31-positive brain microvascular endothelial cells, whereas this increase was substantially attenuated following YNK-H treatment. A parallel increase in QRICH1 expression was also observed in PDGFR-β-positive pericytes in the model rats. Notably, YNK-H treatment similarly attenuated QRICH1 upregulation in pericytes. Collectively, these in vivo findings show that CIRI upregulates QRICH1 in both CD31-positive BMECs and adjacent PDGFR-β-positive pericytes, alongside activation of the upstream PERK/eIF2α cascade, and that YNK-H reverses QRICH1 overactivation in both compartments. Given the central role of BMECs in BBB integrity, subsequent experiments focused on this endothelial compartment.

3.4 YNK directly inhibits OGD/R-induced ERS, apoptosis and PERK/eIF2α/QRICH1 pathway hyperactivation in bEnd.3 brain microvascular endothelial cells (Fig. 4)

The above in vivo results indicated that BMECs, together with adjacent pericytes, constitute a major cellular compartment of PERK/eIF2α/QRICH1 pathway activation during CIRI. To verify whether YNK exerts direct protective effects on endothelial cells independent of other neurovascular cell types, we established an in vitro OGD/R injury model using mouse bEnd.3 cerebral microvascular endothelial cells, with the selective PERK inhibitor GSK2656157 as positive pathway control.

qPCR transcriptional profiling of target genes demonstrated severe endothelial dysfunction after OGD/R insult: synaptic marker Dlg4 was downregulated, pro-apoptotic Bax and Casp3 upregulated, and anti-apoptotic Bcl2 suppressed (**p < 0.01, ***p < 0.001 vs. Control, Fig. 4A-D). YNK-H serum treatment significantly restored Dlg4 expression, elevated Bcl2 mRNA, and repressed Bax and Casp3 transcription (#p < 0.05, ###p < 0.001 vs. OGD/R Model), recapitulating the in vivo anti-apoptotic and synaptoplastic regulatory phenotypes. For ERS pathway genes, OGD/R markedly induced Eif2ak3, Eif2a, Qrich1 and Ddit3 mRNA accumulation (***p < 0.001 vs. Control), while YNK-H downregulated all four transcripts (###p < 0.001 vs. OGD/R Model, Fig. 4E-H). Notably, the protective transcriptional modulation exerted by YNK-H was comparable to that of the pharmacological PERK inhibitor GSK2656157, supporting the involvement of the PERK signaling branch in the effects of YNK, although genetic target validation was not performed.

CD31 immunofluorescence validated pure endothelial identity of cultured bEnd.3 cells (Fig. 4I). BIP co-staining with p-PERK, p-eIF2α and QRICH1 revealed minimal protein co-localization under normoxic Control conditions; OGD/R induced robust cytoplasmic co-localization of ERS marker BIP with phosphorylated PERK, phosphorylated eIF2α and QRICH1. YNK-H intervention drastically reduced the co-localization intensity of these pathway proteins, consistent with qPCR transcriptional data (Fig. 4J-L). Together, these findings show that YNK treatment was associated with reduced OGD/R-induced changes in ER-stress markers and PERK/eIF2α/QRICH1-related readouts in bEnd.3 cells. GSK2656157 produced changes in a similar direction, consistent with possible involvement of PERK signaling.

Discussion

This study provides a preliminary evaluation of the neurovascular protective effects of YNK, a classic TCM formula with long-term clinical application for ischemic stroke, against CIRI. To ensure the scientific rigor of subsequent mechanistic investigations and optimize the therapeutic regimen, we first performed a comprehensive dose-time effect screening experiment. A total of 140 male SD rats were randomly assigned to the Sham, Model and YNK treatment arms and received 7 consecutive days of intragastric pre-administration (low- or high-dose YNK, or an equal volume of normal saline for the Sham and Model groups) before MCAO surgery. After modeling, the rats were then further assigned to 24 h and 72 h reperfusion subgroups—including the model rats, which were divided into IR24 h and IR72 h subgroups at this point—thereby yielding seven experimental groups for evaluating the time-dependent protective effects of YNK. Based on the screening results, YNK-H and 72 h reperfusion were selected as the optimal conditions for subsequent mechanistic experiments. Consistent with these screening outcomes, YNK not only alleviated neurological deficits and reduced cerebral infarct volume in MCAO rats, but also

preserved neuronal morphology and synaptic plasticity by upregulating PSD-95 and BDNF expression [26].

Further molecular detection revealed that YNK exerts multi-dimensional protective activity against CIRI. Biochemical and qPCR data confirmed that YNK significantly improves antioxidant capacity and suppresses the overexpression of pro-inflammatory cytokines in ischemic brain tissue. Meanwhile, YNK restores the balance of apoptosis-regulatory proteins, reduces the number of TUNEL-positive degenerative neurons, and alleviates ischemia-reperfusion induced neuronal damage. All these coordinated effects jointly stabilize the disrupted microenvironment of the ischemic penumbra and create favorable conditions for subsequent neuronal functional repair.

The main finding of this research is that the PERK/eIF2α/QRICH1 endoplasmic reticulum stress signaling axis in brain microvascular endothelial cells is a candidate molecular target associated with the effects of YNK; however, target validation is incomplete. QRICH1 has so far been characterized mainly as a downstream effector that dictates the outcome of unresolved ER stress, while its expression profile and pathological function in cerebral endothelial cells under ischemic conditions remain largely unexplored. Our in vivo immunofluorescence results demonstrated that CIRI induces robust QRICH1 overexpression in both CD31-positive endothelial cells and adjacent pericytes, and that this upregulation was associated with excessive activation of the upstream PERK/eIF2α cascade. Accumulated QRICH1 is reported to exacerbate ER proteotoxic stress and promote endothelial apoptosis, which may contribute to BBB breakdown and subsequent secondary neuronal injury. YNK treatment was associated with attenuated hyperactivation of this signaling cascade in both the ischemic cortex of MCAO rats and cultured bEnd.3 endothelial cells. In vitro assays using the PERK-specific inhibitor GSK2656157 as positive control further supported YNK's specific suppression of PERK signaling, identifying the endothelial PERK/eIF2α/QRICH1 axis as a candidate therapeutic target for reperfusion-induced brain injury.

Most previous pharmacological studies on stroke-related TCM compounds merely focused on direct neuronal protection, ignoring endothelial damage—the upstream initiating event prior to widespread neuronal death. Distinct from such research frameworks, the present study centers on brain microvascular endothelial cells, the core functional constituent of the neurovascular unit. We confirmed that YNK provides broad-spectrum neurovascular protection that is consistent with, and in isolated endothelial cells is accompanied by, alleviation of ERS. Endoplasmic reticulum stress acts as an upstream central hub that governs downstream oxidative stress, neuroinflammation, neuronal apoptosis and synaptic dysfunction. YNK-mediated endothelial protection might help preserve BBB integrity and cerebral microcirculatory perfusion, thereby potentially mitigating secondary neuronal damage within the ischemic penumbra; however, BBB integrity and perfusion were not directly measured in this study. This endothelial-centered mechanistic interpretation better explains the multi-target advantages of multi-component TCM formulas, and aligns with the classical TCM therapeutic principle of activating blood circulation and unblocking collaterals to improve cerebral microcirculation.

Another feature of this work is the multi-level evidence framework constructed by in vivo phenotypic screening, tissue-level cellular localization and isolated endothelial in vitro functional verification. In vivo immunofluorescence localized hyperactivated PERK/eIF2α/QRICH1 signaling to cerebral microvascular endothelial cells and adjacent pericytes. Follow-up experiments on isolated bEnd.3 cells excluded interference from neurons, glia and other brain-resident cells, showing that YNK-containing serum was associated with changes in bEnd.3 cells cultured without other neurovascular cell types. This multi-layer experimental design reduces, but does not eliminate, the ambiguity of purely in vivo stroke research and provides cell-level evidence for the vascular effects of YNK; definitive target validation will require genetic and active-constituent studies.

Mechanistically, persistent unresolved ERS in BMECs integrates oxidative stress, inflammatory responses and apoptotic signaling to jointly amplify CIRI pathological damage[27, 28]. Importantly, ERS interacts with ROS and inflammatory mediators to exacerbate cell death; thus, YNK's ERS-mitigating property acts as a core hub underlying its multi-level neuroprotective capacity [29].

At the cellular level, YNK improves neuronal viability by inhibiting apoptotic cascades. The elevated Bcl-2/Bax ratio and suppressed Caspase-3 abundance in the ischemic penumbra indicate blocked ERS-mediated apoptotic signaling. Histological and immunofluorescence analyses further confirmed reduced neuronal pyknosis, demonstrating that YNK's neuroprotective benefits originate from both direct neuronal stabilization and indirect support via maintained vascular integrity. Moreover, elevated synaptic marker expression implies improved long-term functional recovery after CIRI [30], reinforcing the intrinsic connection between neurovascular protection, ERS relief and neuronal plasticity [31].

Most importantly, our findings show that YNK's neurovascular protection is associated with suppression of PERK/eIF2α/QRICH1-mediated ERS in BMECs, and that in isolated endothelial cells this suppression parallels the effect of pharmacological PERK inhibition[32]. Hyperactivation of the PERK/eIF2α/QRICH1 axis has been reported to drive endothelial ROS accumulation, pro-inflammatory factor secretion and programmed cell death; these pathological processes were attenuated in the YNK-treated groups in the present models. Beyond endothelial ERS inhibition, YNK treatment was accompanied by preserved PSD-95 and BDNF levels, suggesting potential benefits for long-term neurological recovery post-stroke. As a multi-ingredient formula, YNK may simultaneously modulate multiple interconnected pathological cascades, which is consistent with the complex multifactorial nature of CIRI. The quality-control markers calycosin glucoside and ononin were not tested individually, and their contribution to the observed bioactivities remains unknown; isolation and functional verification of single active monomers are required [33].

Extensive molecular crosstalk exists between ERS and other pathological pathways such as autophagy, ferroptosis and synaptic remodeling under hypoxic-ischemic conditions [34, 35]. The anti-apoptotic and synaptoprotective effects of YNK observed in this study may stem from both direct suppression of the PERK/eIF2α/QRICH1 axis and indirect regulation of these interconnected signaling networks, ultimately generating synergistic neurovascular protective outcomes[36].

Despite these promising findings, several limitations should be acknowledged to guide subsequent investigation. First, YNK is a multi-component herbal preparation. Although its quality was controlled by HPLC quantification of four marker compounds, comprehensive chemical characterization and identification of the specific bioactive constituent(s) responsible for the observed neuroprotective effects were not performed; the attribution of effects to YNK as a formula rather than to defined compounds therefore remains provisional. Second, YNK-only control groups were not included in either the in vivo or in vitro experiments. We cannot exclude baseline effects of YNK or YNK-containing serum on the measured parameters in the absence of ischemic/OGD injury, and the injury-specific nature of the effects requires confirmation. Third, although the MCAO procedure followed the intraluminal filament method, cerebral blood flow was not monitored by Laser Doppler flowmetry, and procedure-related mortality, postoperative monitoring/care, surgical failures and predefined exclusion criteria were not fully recorded or reported; this limits assessment of model rigor and reproducibility. Fourth, only pharmacological PERK inhibition was used for in vitro validation; endothelial-specific PERK or QRICH1 knockout animal models are required to confirm the cell-autonomous pathological function of this signaling axis in BMECs in vivo. Fifth, the bidirectional regulatory crosstalk between QRICH1, ferroptosis and autophagy during YNK-mediated ERS alleviation has not been fully clarified, which requires multi-omics profiling to systematically map the relevant regulatory network. Finally, the individual active ingredients of YNK responsible for PERK pathway inhibition and their synergistic interactions remain unisolated and unquantified, requiring further phytochemical separation and functional verification of monomer compounds. Transcriptomic and proteomic profiling of YNK-treated endothelial cells will further unravel its systematic multi-target regulatory network against CIRI.

Collectively, this study provides preliminary evidence that the neurovascular protective effects of YNK against CIRI are accompanied by suppression of PERK/eIF2α/QRICH1-mediated ERS in BMECs. The endothelial PERK/eIF2α/QRICH1 axis is proposed as a candidate therapeutic target that requires validation by genetic and active-constituent studies before clinical evaluation of YNK can be considered.

Conclusions

This study provides preliminary evidence for a protective effect of YNK against CIRI, focusing primarily on BMECs. YNK reduced cerebral infarct volume and improved neurological deficits in MCAO rats. These effects were accompanied by reduced oxidative stress, neuroinflammation and neuronal apoptosis, and in isolated bEnd.3 cells by suppression of PERK/eIF2α/QRICH1-mediated ERS comparable to pharmacological PERK inhibition. Because no genetic loss-of-function, CBF monitoring, YNK-only control groups, or active-constituent identification were included, these data support, but do not establish, a causal role of the endothelial PERK/eIF2α/QRICH1 axis in CIRI. YNK also attenuated ischemia-induced QRICH1 upregulation in cerebral microvascular pericytes, concurrently with its endothelial effects, suggesting a possible effect across the neurovascular unit. These findings are hypothesis-generating and provide a rationale, rather than definitive preclinical evidence, for further evaluation of YNK in ischemic stroke; the endothelial PERK/eIF2α/QRICH1 pathway warrants validation in genetic and active-constituent studies.

Declarations

Ethics approval and consent to participate

The animal experiment protocol was approved by the Animal Ethics Committee of Guangzhou University of Chinese Medicine (Approval No. : 20251201003) and omplied with the National Institutes of Health Guide for the Care and Use of Laboratory Animals. Consent to participate: Not applicable; no human participants were involved.

Patient consent for publication

Clinical trial number: not applicable.

Conflict of Interest

The authors declare no competing financial or non-financial interests.

Funding

This work was supported by Basic and Applied Basic Research Foundation of Guangdong Province (No. 2023B1515120075), Science and Technology Projects in Guangzhou (No. 2025A03J4066;No. 2025A03J4077), and Guangdong Provincial Key Laboratory of Research on Emergency in TCM (No. 2023B1212060062).

Author Contribution

J.-P. Xu performed the experiments, collected samples and acquired experimental data, analyzed and statistically processed the raw data, visualized the results, prepared figures and tables, and drafted the manuscript. M.-H. Zheng prepared figures and tables and supervised the research. D.X. prepared figures and tables and supervised the research. H.T. improved the language and logical structure of the manuscript and supervised the research. Q.-H. Lv and J. Ouyang processed raw data and visualized the results. X.-Y. Xu, D.W. and Y.-H. Qiu collected samples and acquired experimental data. J.-Y. Zheng conceived the study and provided supervision. Y.-F. Cai acquired funding and managed the research project. S.-J. Zhang supervised the research and managed the research project. All authors read and approved the final manuscript.

Acknowledgement

This study was supported by the Department of Neurology, The Second Clinical College of Guangzhou University of Chinese Medicine, and Guangdong Provincial Key Laboratory of Syndrome and Formula, School of Pharmaceutical Sciences, Guangzhou University of Chinese Medicine. We thank all team members for their technical support during experiments and data analysis.

Availability of data and materials

All data generated or analyzed during this study are included in this published article and its supplementary information files. Further inquiries can be directed to the corresponding authors.

References

1. Hilkens NA, Casolla B, Leung TW, De Leeuw FE, Stroke (2024) Lancet 403(10446):2820–2836. 10.1016/S0140-6736(24)00642-1
2. Guo Mmin, Qu S, biao, Lu H ling, Wang W bo, He ML, Su JL, Chen J, Wang Y (2021) Biochanin A Alleviates Cerebral Ischemia/Reperfusion Injury by Suppressing Endoplasmic Reticulum Stress-Induced Apoptosis and p38MAPK Signaling Pathway In Vivo and In Vitro. Front Endocrinol. ;12:646720. 10.3389/fendo.2021.646720
3. Zhang M, Liu Q, Meng H, Duan H, Liu X, Wu J, Gao F, Wang S, Tan R, Yuan J (2024) Ischemia-reperfusion injury: molecular mechanisms and therapeutic targets. Sig Transduct Target Ther 9(1):12. 10.1038/s41392-023-01688-x
4. Iadecola C (2017) The Neurovascular Unit Coming of Age: A Journey through Neurovascular Coupling in Health and Disease. Neuron 96(1):17–42. 10.1016/j.neuron.2017.07.030
5. Li Y, Li M, Feng S, Xu Q, Zhang X, Xiong X, Gu L (2024) Ferroptosis and endoplasmic reticulum stress in ischemic stroke. Neural Regeneration Res 19(3):611–618. 10.4103/1673-5374.380870
6. Van Splunder H, Villacampa P, Martínez-Romero A, Graupera M (2024) Pericytes in the disease spotlight. Trends Cell Biol 34(1):58–71. 10.1016/j.tcb.2023.06.001
7. Hu S, Fei Y, Jin C, Yao J, Ding H, Wang J, Liu C (2024) Ginsenoside Rd enhances blood-brain barrier integrity after cerebral ischemia/reperfusion by alleviating endothelial cells ferroptosis via activation of NRG1/ErbB4-mediated PI3K/Akt/mTOR signaling pathway. Neuropharmacology 251:109929. 10.1016/j.neuropharm.2024.109929 PubMed PMID: 38521230
8. Liu C, Sui H, Li Z, Sun Z, Li C, Chen G, Ma Z, Cao H, Xi H (2025) THBS1 in macrophage-derived exosomes exacerbates cerebral ischemia-reperfusion injury by inducing ferroptosis in endothelial cells. J Neuroinflammation 22(1):48. 10.1186/s12974-025-03382-x PubMed PMID: 39994679; PubMed Central PMCID: PMC11854006
9. Wang L, Li J, Wang Y, Ge C, Huang Q, Li L, Wang N, Chen Y, Zhou X, Chang D, Li D, Hou J (2023) Dan-Deng-Tong-Nao softgel capsule promotes angiogenesis of cerebral microvasculature to protect cerebral ischemia reperfusion injury via activating HIF-1α-VEGFA-Notch1 signaling pathway. Phytomedicine 118:154966. 10.1016/j.phymed.2023.154966 PubMed PMID: 37487254

10. Zeng F, Cao J, Hong Z, Liu Y, Hao J, Qin Z, Zou X, Tao T (2023) Single-cell analyses reveal the dynamic functions of Itgb2 + microglia subclusters at different stages of cerebral ischemia-reperfusion injury in transient middle cerebral occlusion mice model. Front Immunol 14:1114663. 10.3389/fimmu.2023.1114663 PubMed PMID: 37063847; PubMed Central PMCID: PMC10098327
11. Zhang W, Han L, Wen Y, Su L, Li Y, Luo X (2023) Electroacupuncture reverses endothelial cell death and promotes angiogenesis through the VEGF/Notch signaling pathway after focal cerebral ischemia-reperfusion injury. Brain Behav 13(3):e2912. 10.1002/brb32912 PubMed PMID: 36786352; PubMed Central PMCID: PMC10013937
12. Jiang H, Zhang C, Lin M, Yin Y, Deng S, Liu W, Zhuo B, Tian G, Du Y, Meng Z (2024) Deciphering the mechanistic impact of acupuncture on the neurovascular unit in acute ischemic stroke: Insights from basic research in a narrative review. Ageing Res Rev 101:102536. 10.1016/j.arr.2024.102536 PubMed PMID: 39384155
13. Wang Q, Zheng J, Pettersson S, Reynolds R, Tan EK (2023) The link between neuroinflammation and the neurovascular unit in synucleinopathies. Sci Adv 9(7):eabq1141. 10.1126/sciadv.abq1141 PubMed PMID: 36791205; PubMed Central PMCID: PMC9931221
14. Vrselja Z, Daniele SG, Silbereis J, Talpo F, Morozov YM, Sousa AMM, Tanaka BS, Skarica M, Pletikos M, Kaur N, Zhuang ZW, Liu Z, Alkawadri R, Sinusas AJ, Latham SR, Waxman SG, Sestan N (2019) Restoration of brain circulation and cellular functions hours post-mortem. Nature 568(7752):336–343. 10.1038/s41586-019-1099-1
15. Erickson MA, Banks WA (2018) Neuroimmune Axes of the Blood–Brain Barriers and Blood–Brain Interfaces: Bases for Physiological Regulation, Disease States, and Pharmacological Interventions. Pharmacol Rev 70(2):278–314. 10.1124/pr.117.014647
16. Wang P, Liu J, Zhang M, Yang J, Lian P, Cheng X, Qin J (2025) Radiation exposure induced blood-brain barrier injury via mitochondria-mediated sterile inflammation [Internet]. Neuroscience; [cited 2026 Sep 28]. Available from: http://biorxiv.org/lookup/doi/10.1101/2025.02.03.636229 doi:10.1101/2025.02.03.636229
17. Thaunat O (2024) Natural killer cell-mediated innate microvascular rejection. Nat Rev Nephrol 20(8):489–490. 10.1038/s41581-024-00862-w PubMed PMID: 38898355
18. Hetz C, Chevet E, Oakes SA (2015) Proteostasis control by the unfolded protein response. Nat Cell Biol 17(7):829–838. 10.1038/ncb3184
19. Yu X, Dang L, Zhang R, Yang W (2024) Therapeutic Potential of Targeting the PERK Signaling Pathway in Ischemic Stroke. Pharmaceuticals 17(3). 10.3390/ph17030353
20. Wang L, Liu Y, Zhang X, Ye Y, Xiong X, Zhang S, Gu L, Jian Z, Wang H (2022) Endoplasmic Reticulum Stress and the Unfolded Protein Response in Cerebral Ischemia/Reperfusion Injury. Front Cell Neurosci 16. 10.3389/fncel.2022.864426
21. Emam AM, Saad MA, Ahmed NA, Zaki HF (2021) Vortioxetine mitigates neuronal damage by restricting PERK/eIF2α/ATF4/CHOP signaling pathway in rats subjected to focal cerebral ischemia-reperfusion. Life Sci 283:119865. 10.1016/j.lfs.2021.119865

22. Wu Y, Fan X, Chen S, Deng L, Jiang L, Yang S, Dong Z (2022) Geraniol-Mediated Suppression of Endoplasmic Reticulum Stress Protects against Cerebral Ischemia–Reperfusion Injury via the PERK-ATF4-CHOP Pathway. Int J Mol Sci 24(1). 10.3390/ijms24010544
23. You K, Wang L, Chou CH, Liu K, Nakata T, Jaiswal A, Yao J, Lefkovith A, Omar A, Perrigoue JG, Towne JE, Regev A, Graham DB, Xavier RJ (2021) QRICH1 dictates the outcome of ER stress through transcriptional control of proteostasis. Science 371(6524):eabb6896. 10.1126/science.abb6896
24. Dirnagl U, Iadecola C, Moskowitz MA (1999) Pathobiology of ischaemic stroke: an integrated view. Trends Neurosci 22(9):391–397. 10.1016/S0166-2236(99)01401-0
25. Wen GQ, Chen J, Li J, Huang Y, Li X, He S, Li Y, Wang L, Li Z, Li P (2022) Establishment of fingerprint of Yinaokang extract and content determination of 4 components. Chin J Hosp Pharm 42(13):1311–1315
26. Lv H, Li Y, Cheng Q, Chen J, Chen W (2021) Neuroprotective Effects Against Cerebral Ischemic Injury Exerted by Dexmedetomidine via the HDAC5/NPAS4/MDM2/PSD-95 Axis. Mol Neurobiol 58(5):1990–2004. 10.1007/s12035-020-02223-7
27. Chen X, Shi C, He M, Xiong S, Xia X (2023) Endoplasmic reticulum stress: molecular mechanism and therapeutic targets. Sig Transduct Target Ther 8(1):352. 10.1038/s41392-023-01570-w
28. Nakka VP, Gusain A, Raghubir R (2010) Endoplasmic Reticulum Stress Plays Critical Role in Brain Damage After Cerebral Ischemia/Reperfusion in Rats. Neurotox Res 17(2):189–202. 10.1007/s12640-009-9110-5
29. Ron D, Walter P (2007) Signal integration in the endoplasmic reticulum unfolded protein response. Nat Rev Mol Cell Biol 8(7):519–529. 10.1038/nrm2199
30. Xie G, Song C, Lin X, Yang M, Fan X, Liu W, Tao J, Chen L, Huang J (2019) Electroacupuncture Regulates Hippocampal Synaptic Plasticity via Inhibiting Janus-Activated Kinase 2/Signal Transducer and Activator of Transcription 3 Signaling in Cerebral Ischemic Rats. J Stroke Cerebrovasc Dis 28(3):792–799. 10.1016/j.jstrokecerebrovasdis.2018.11.025
31. Li C, Ke C, Su Y, Wan C (2021) Exercise Intervention Promotes the Growth of Synapses and Regulates Neuroplasticity in Rats With Ischemic Stroke Through Exosomes. Front Neurol 12:752595. 10.3389/fneur.2021.752595
32. Zheng W, Wang K, Wu Y, Yan G, Zhang C, Li Z, Wang L, Chen S (2022) C9orf72 regulates the unfolded protein response and stress granule formation by interacting with eIF2α. Theranostics 12(17):7289–7306. 10.7150/thno.76138 PubMed PMID: 36438488; PubMed Central PMCID: PMC9691347
33. Zhu T, Wang L, Wang L, ping, Wan Q (2022) Therapeutic targets of neuroprotection and neurorestoration in ischemic stroke: Applications for natural compounds from medicinal herbs. Biomed Pharmacother 148:112719. 10.1016/j.biopha.2022.112719
34. Sano R, Reed JC (2013) ER stress-induced cell death mechanisms. Biochimica et Biophysica Acta (BBA) -. Mol Cell Res 1833(12):3460–3470. 10.1016/j.bbamcr.2013.06.028
35. Yin Y, Sun G, Li E, Kiselyov K, Sun D (2017) ER stress and impaired autophagy flux in neuronal degeneration and brain injury. Ageing Res Rev 34:3–14. 10.1016/j.arr.2016.08.008

36. Alsbrook DL, Di Napoli M, Bhatia K, Biller J, Andalib S, Hinduja A, Rodrigues R, Rodriguez M, Sabbagh SY, Selim M, Farahabadi MH, Jafarli A, Divani AA (2023) Neuroinflammation in Acute Ischemic and Hemorrhagic Stroke. Curr Neurol Neurosci Rep 23(8):407–431. 10.1007/s11910-023-01282-2

Figures

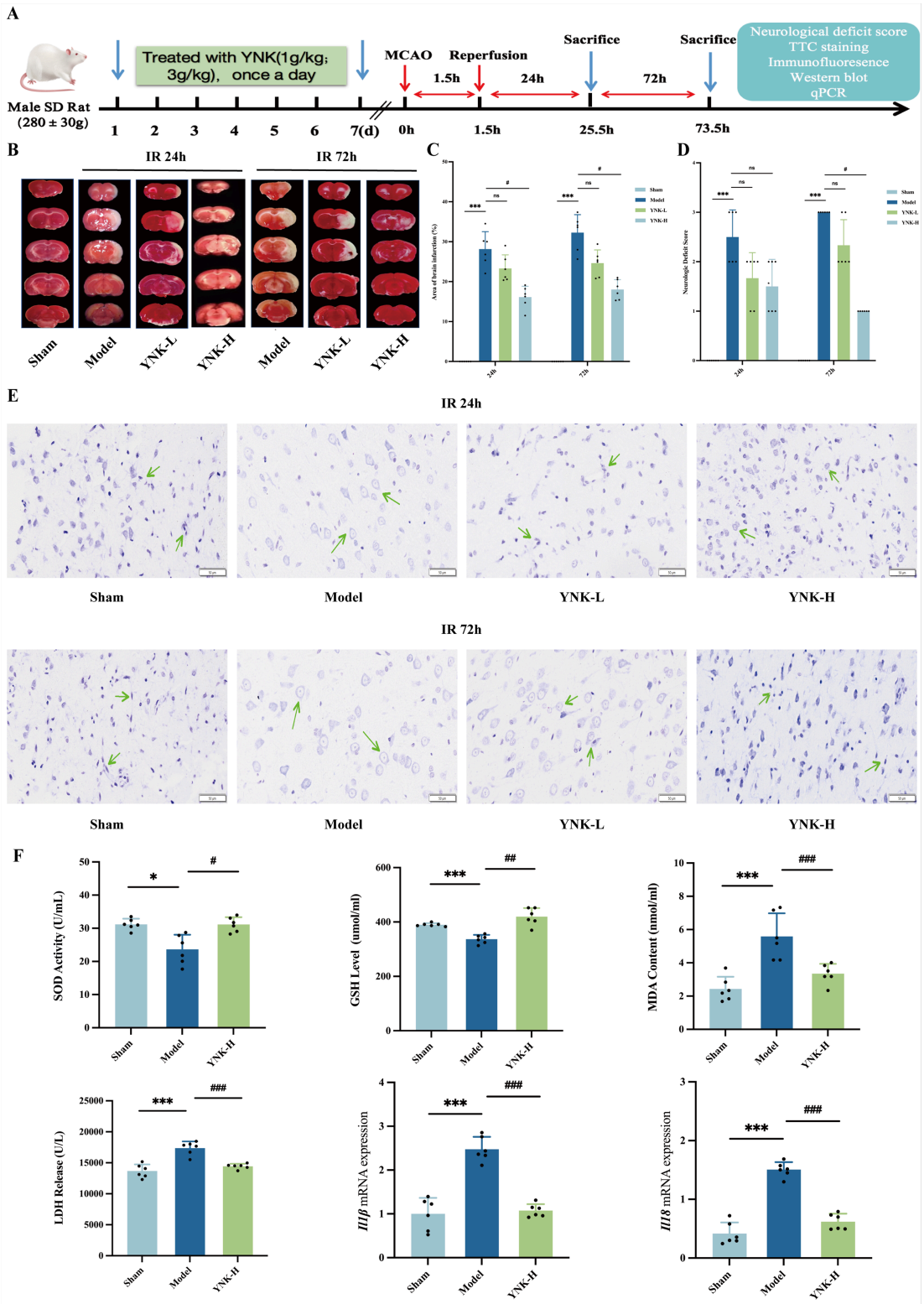


Figure 1

YNK alleviates cerebral ischemia-reperfusion injury, neurological dysfunction, neuronal loss, oxidative stress and neuroinflammation in MCAO rats

(**A**) Schematic timeline of animal grouping, YNK administration, MCAO operation, reperfusion time points and sample detection indicators. Male SD rats received intragastric YNK (1 g/kg for low dose, YNK-L; 3 g/kg for high dose, YNK-H) once daily for 7 consecutive days before 90-min MCAO occlusion, followed by 24 h or 72 h reperfusion for subsequent detection. (**B**) Representative TTC-stained coronal brain slices from Sham, IR24 h Model, IR24 h YNK-L, IR24 h YNK-H, IR72 h Model, IR72 h YNK-L and IR72 h YNK-H groups. Pale white areas represent cerebral infarct lesions. (**C**) Quantitative statistical analysis of cerebral infarct volume percentage at 24 h and 72 h after reperfusion.

(**D**) Quantitative statistical analysis of neurological deficit scores evaluated by Zea Longa scale at 24 h and 72 h after reperfusion; higher scores indicate more severe neurological impairment. (**E**) Representative Nissl staining micrographs of cortical ischemic penumbra tissues at IR24 h and IR72 h time points. Green arrows indicate damaged, pyknosis neurons. Scale bar is marked on each micrograph. (**F**) Biochemical detection of oxidative stress indicators and qPCR quantification of pro-inflammatory cytokines in IR72 h brain tissues. Subgraphs sequentially display: SOD activity, GSH level, MDA content, serum LDH release, Il1β mRNA expression, Il18 mRNA expression. Data are presented as mean ± SEM (n = 6 per group). *p < 0.05 vs. Sham group; ***p < 0.001 vs. Sham group; #p < 0.05, ##p < 0.01, ###p < 0.001 vs. IR72 h Model group; ns, no statistical significance.

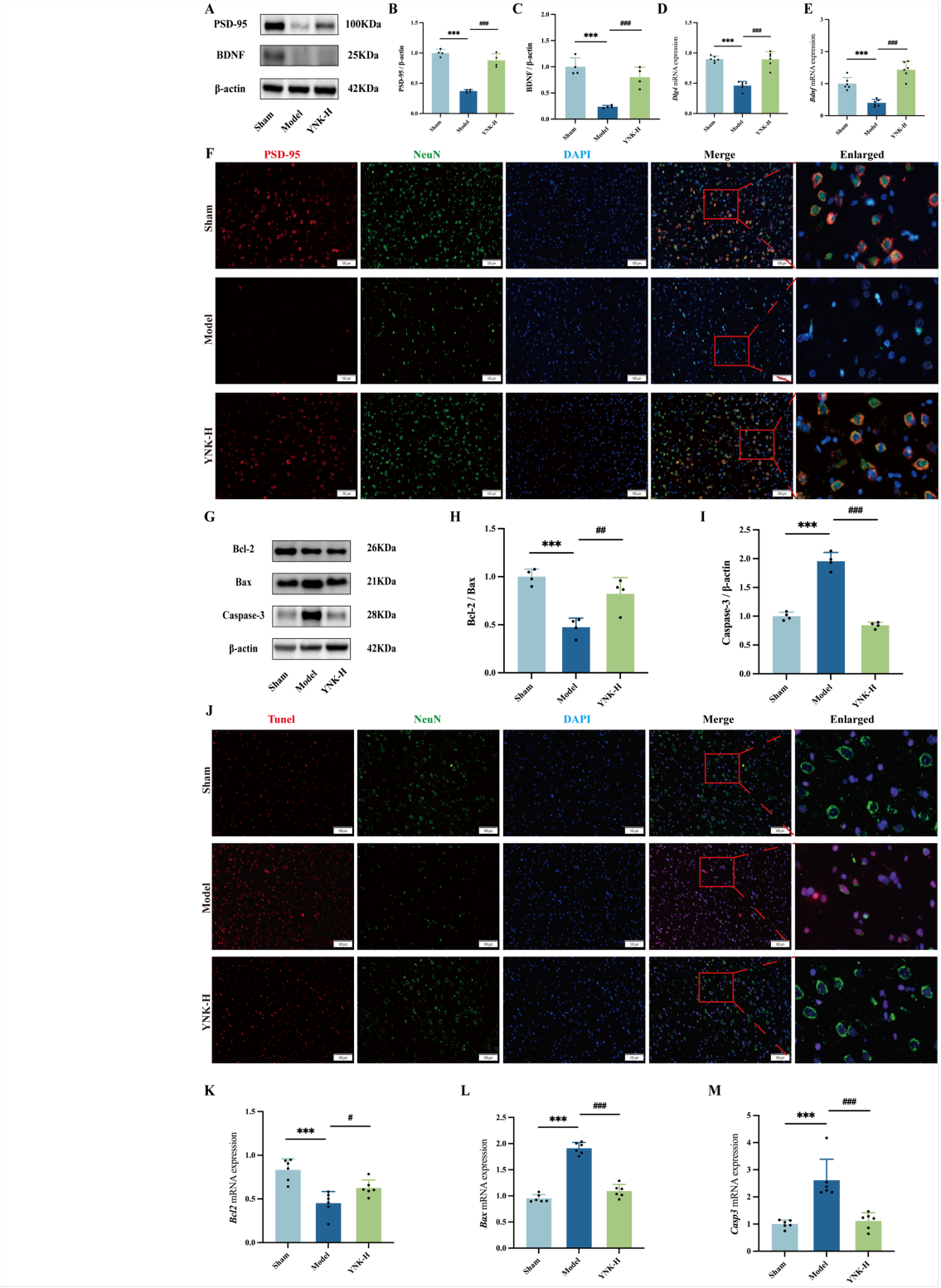


Figure 2

YNK rescues impaired synaptic plasticity and alleviates neuronal apoptosis in the cortical ischemic penumbra of MCAO rats

(**A**) Representative western blot bands of synaptic plasticity-related proteins PSD-95 and BDNF, with β-actin as internal reference, from Sham, IR72 h Model and YNK-H groups. (**B-E**) Quantitative analysis of

synaptic markers: (**B**) PSD-95/β-actin protein level, (**C**) BDNF/β-actin protein level, (**D**) Dlg4 mRNA expression, (**E**) Bdnf mRNA expression. (**F**) Double immunofluorescence co-staining of PSD-95 (red) and pan-neuronal marker NeuN (green) in ischemic cortex; nuclei were labeled with DAPI (blue). Merged images and partial enlarged views display PSD-95 expression in neurons. Scale bar = 50 μm. (**G**) Representative western blot bands of apoptosis-related proteins Bcl-2, Bax, Caspase-3 and reference β-actin. (**H-I**) Quantitative gray analysis of apoptotic proteins: (**H**) Bcl-2/Bax ratio, (**I**) Caspase-3/β-actin relative expression. (**J**) TUNEL (apoptotic cell marker, red) and NeuN (neuron, green) co-staining immunofluorescence micrographs. DAPI stains cell nuclei; merged and enlarged fields show apoptotic neuron number changes. Scale bar = 100 μm. (**K-M**) qPCR detection of apoptosis-associated gene transcription levels: (**K**) Bcl2, (**L**) Bax, (**M**) Casp3. Data are presented as mean ± SEM (n = 6 per group). ***p < 0.001 vs. Sham group; #p < 0.05, ##p < 0.01, ###p < 0.001 vs. IR72 h Model group.

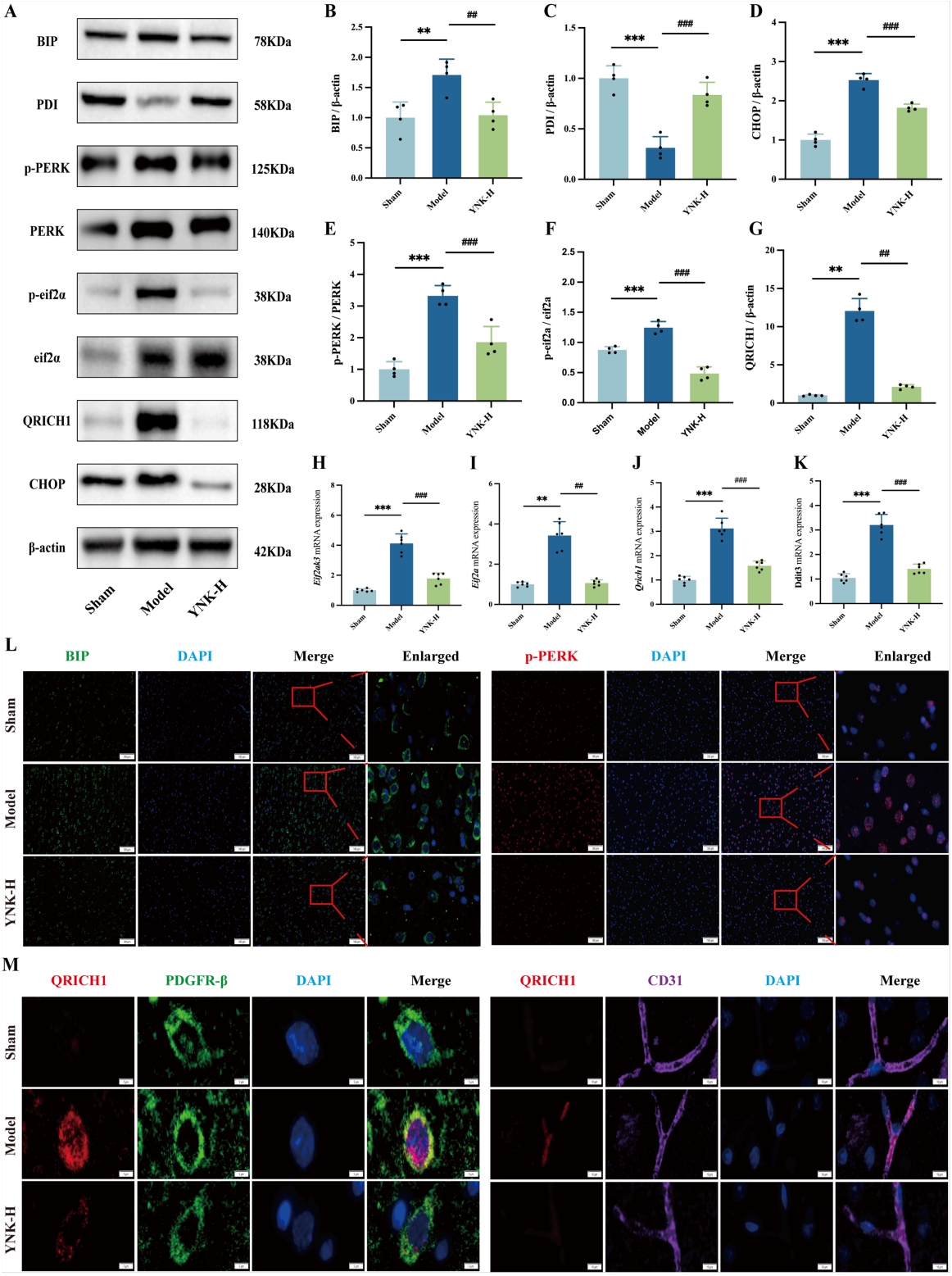


Figure 3

YNK inhibits PERK/eIF2α/QRICH1-mediated endoplasmic reticulum stress (ERS) in the cerebral cortex of MCAO rats and alleviates QRICH1 expression in cerebral microvascular endothelial cells and pericytes

(**A**) Representative western blot bands of ERS marker proteins (BIP, PDI, CHOP), core pathway proteins (p-PERK, PERK, p-eIF2α, eIF2α, QRICH1) and internal reference β-actin in cortical ischemic penumbra of Sham**,** Model (IR72 h) and YNK-H groups. (**B-G**) Quantitative gray value analysis of western blot bands: (**B**) BIP/β-actin, (**C**) PDI/β-actin, (**D**) CHOP/β-actin, (**E**) p-PERK/PERK phosphorylation ratio, (**F**) p-eIF2α/eIF2α phosphorylation ratio, (**G**) QRICH1/β-actin. (**H-K**) qPCR detection of mRNA expression of ERS and PERK pathway-related genes: (**H**) Eif2ak3 (PERK), (**I**) Eif2a, (**J**) Qrich1, (**K**) Ddit3 (CHOP). (**L**) Immunofluorescence single staining of ERS marker BIP (green) and phosphorylated PERK (p-PERK, red) in ischemic cortex; cell nuclei were counterstained with DAPI (blue). Merged images and local enlarged fields are displayed on the right. Scale bar = 100 μm. (**M**) Double immunofluorescence co-localization of QRICH1 with pericyte marker PDGFR-β (upper row), and QRICH1 with endothelial marker CD31 (lower row). Nuclei were stained with DAPI (blue). Merged and enlarged views demonstrate cellular localization of QRICH1. Scale bar = 5 μm. Data are presented as mean ± SEM (n = 6 per group). **p < 0.01, ***p < 0.001 vs. Sham group; ##p < 0.01, ###p < 0.001 vs. IR72 h Model group.

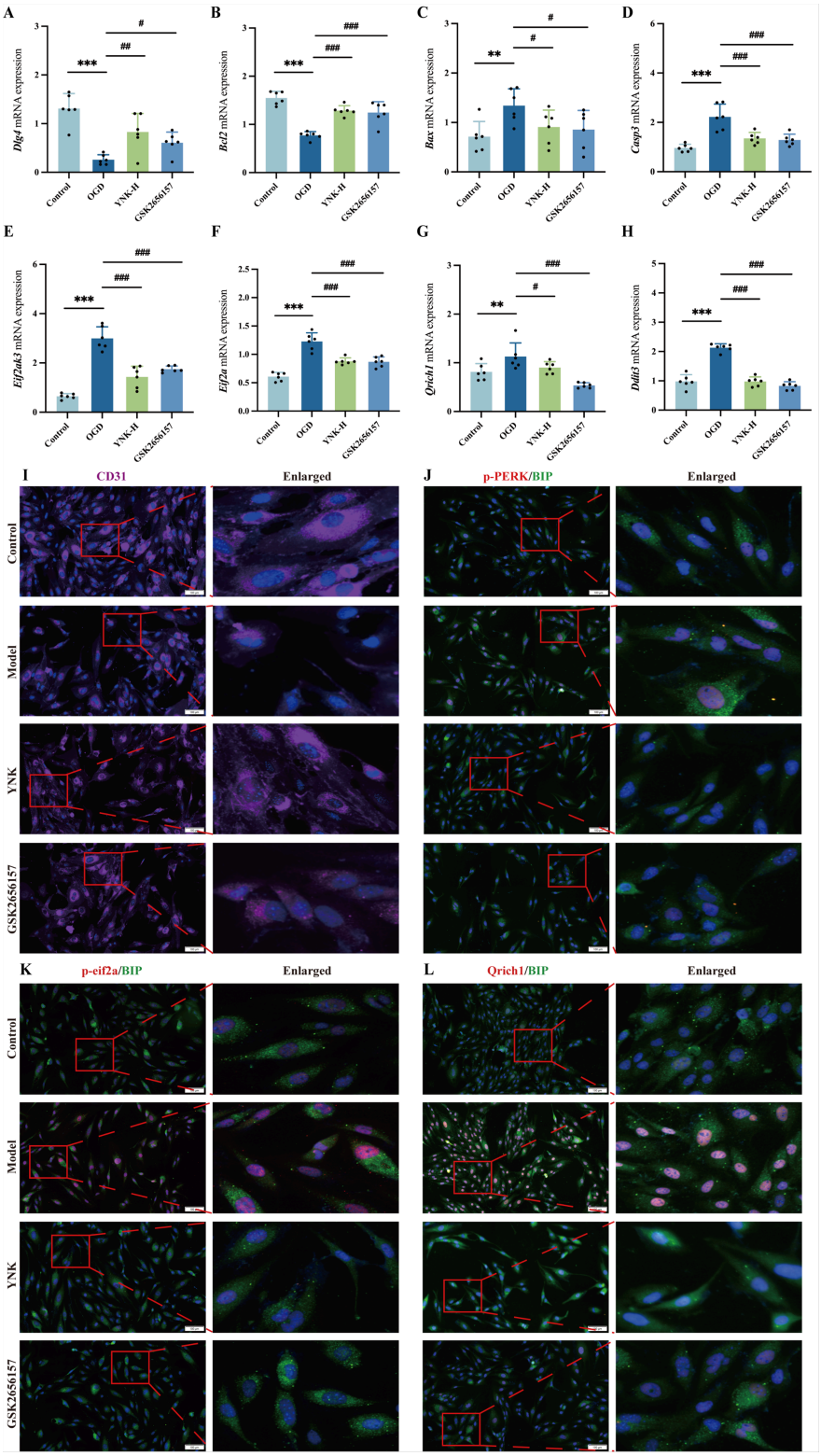


Figure 4

YNK suppresses OGD/R-triggered apoptosis and PERK/eIF2α/QRICH1 ERS pathway overactivation in bEnd.3 mouse brain microvascular endothelial cells, with the PERK inhibitor GSK2656157 as positive control (A-H)

qPCR quantification of target gene mRNA expression in bEnd.3 cells under Control, OGD/R Model, YNK-H and GSK2656157 intervention groups: (**A**) Dlg4 (PSD-95, synaptic marker), (**B**) anti-apoptotic gene Bcl2, (**C**) pro-apoptotic gene Bax, (**D**) apoptotic executive gene Casp3, (**E**) Eif2ak3, (**F**) Eif2a, (**G**) Qrich1, (**H**) Ddit3. (**I**) Immunofluorescence staining of endothelial specific marker CD31 (purple) to identify bEnd.3 cell identity; local enlarged areas are shown on the right. Scale bar = 100 μm. (**J-L**) Double immunofluorescence co-staining of ERS marker BIP (green) with pathway proteins in bEnd.3 cells: (**J**) p-PERK (red), (**K**) p-eIF2α (red), (**L**) QRICH1 (red). Cell nuclei were stained by DAPI (blue). Merged images and magnified local regions show co-localization intensity changes of target proteins. Scale bar = 100 μm. Data are presented as mean ± SEM (n = 6 per group). **p < 0.01, ***p < 0.001 vs. Control group; #p < 0.05, ###p < 0.001 vs. OGD/R Model group.

Supplementary Files

This is a list of supplementary files associated with this preprint. Click to download.

- Table1.docx
- Table2.docx
- TableS2.docx
- TableS1.docx
- TableS3.docx
- Supplementarymaterial.zip